Met. Mater. Int., Vol. 17, No. 3 (2011), pp. 485~496
doi: 10.1007/s12540-011-0629-7 Published 29 June 2011

Mathematical Modeling of the Burden Distribution in the Blast Furnace Shaft

Jong-In Park[1], Hun-Je Jung[1], Min-Kyu Jo[1], Han-Sang Oh[2], and Jeong-Whan Han[1,*]

[1]School of Materials Science and Engineering, Inha University, Incheon 402-751, Korea
[2]Technical Research Center, Hyundai Steel, Dangjin-gun, Chungnam 167-32, Korea

(received date: 14 September 2010 / accepted date: 5 January 2011)

Process efficiency in the blast furnace is influenced by the gas flow pattern, which is dictated by the burden profile. Therefore, it is important to control the burden distribution so as to achieve reasonable gas flow in the blast furnace operation. Additionally, the charging pattern selection is important as it affects the burden trajectory and stock profile. For analysis of the burden distribution, a new analysis model was developed by use of the spreadsheet program, Microsoft® Office Excel, based on visual basic. This model is composed of the falling burden trajectory and a stock model. The burden trajectory is determined by the burden type, batch weight, rotating velocity of the chute, tilting angle, and friction coefficient. After falling, stock lines are formed by the angle of repose, which is affected by the burden trajectory and the falling velocity. The mathematical formulas for developing this model were modified by a scaled model experiment and DEM simulation.

Keywords: metals, oxides, cold working, mechanical properties computer simulation

1. INTRODUCTION

A blast furnace (BF) is a heat exchange and reduction reactor involving counter-current flows of gaseous and solid materials. The efficiency of turning iron ore into molten metal is dominated by the heat exchange between gas and charged ore in a solid layer, but essentially depends on the gas flow distribution. That is, the pressure loss, which affects the efficiency of the iron-making process, relies on the burden distribution. Therefore, inefforts to enhance the charging method, the conventionally used charging equipment has been continuously improved and new systems have been developed. The charging equipment, starting from the cup and cone top, has thereby evolved from the first generation of one bell in the late 19th century into the third generation with a bell-less top in the 1970s [1]. With the development of such charging equipment has come the concept of using burden materials to control furnace operation by adjusting the layer thickness of iron ore and the coke layer in the radial direction of the BF instead of by simply putting fuel and material into the BF. In addition, burden distribution models [2-5] based on model experiments have been developed and applied to BF operation.

Iron ore and coke, the representative burden materials in the BF, vary in terms of particle mean size, porosity, and shape factor. It is known that the permeability of coke is 5 times greater than that of iron ore [6]. Consequently, the gas pressure loss in the BF changes according to the average thickness of the coke and iron ore layers. Since the thicknesses of the iron ore and coke layers put into the BF are not constant in the radial direction, the gas pressure loss also varies with respect to the radial direction. Therefore, control of the pressure loss plays a pivotal role in the improvement of operating efficiency.

In this study, the burden trajectory and stock profile, which are affected by the BF operating conditions, are studied by the present analysis model. A visual basic based spreadsheet, Microsoft® Office Excel, was used to develop the analysis model for the falling and stacking of the burden. Spreadsheet models such as the MasMod model, [7] also have been used for analysis of the iron-making process. These models be easily adapted by users, because control and modification of the model is easier than with other commercial packages.

In previous studies, most numerical simulations [8-13] have assumed burden material as a mixed layer of ore and coke. Thus, the influence of the burden distribution has not been sufficiently investigated. To resolve this problem, a specific burden distribution is considered in the present work by classifying the burden type, such as ore large, ore small, coke base, and center coke. Also, the creation of a mixed

*Corresponding author: jwhan@inha.ac.kr

layer due to collapse of the coke layer is added to provide a detailed burden distribution. The burden to be put into the BF has different properties according to the burden type.

The mathematical formula was developed based on experiments using 1/12 and 1/5 scaled models and was modified on the basis of a DEM (Discrete Element Method) simulation [14]. Variables of the model included the charging mode, notch angle, and amount of burden material, all of which are frequently used in real operations. The burden trajectory was calculated by taking into account the frictional force between particles and between particles and the chute and the turning force of the chute. The stock lines were calculated according to different angles of repose due to the calculated burden trajectory and initial variables. The results obtained from this model, such as the stock profile, will be used for the analysis model of the burden descent and gas flow.

2. NUMERICAL METHOD

This analysis model for the burden distribution is composed of a 2-dimensional falling and staking model. The results of the DEM and the 1/12 and 1/5 scaled model experiments are used for the development of mathematical formula. The analysis model was effectively developed via a spreadsheet using Microsoft® Excel. The outputs of the model are the falling trajectory, radial burden profile, particle size distribution, and mixed layer formation due to the penetration of ore into coke near center region.

2.1. Spreadsheet model

Microsoft® Excel has the basic features of all spreadsheets, using a grid of cells arranged in numbered rows and letter-named columns to organize data manipulations, similar to arithmetic operations. It features calculation, graphing tools, pivot tables, and a macro programming language called VBA (Visual Basic for Applications). It has been very widely applied including for numerical analysis of the iron-making process. VBA allows the user to employ a wide variety of numerical methods, for example, in solving differential equations of mathematical physics, [15,16] and then report the results back to the spreadsheet.

The analysis model that runs in the spreadsheet includes a GUI (Graphic User Interface) developed via visual basic coding. The model menu is divided roughly into three parts: calculation conditions, program run, and results. Operators can easily set up boundary conditions such as notch angle, charging pattern, shape of the blast furnace, and burden properties in the calculation condition sections. Also, the results section displays parameters such as charge weight and volume according to the charging pattern, the angle of repose, the thickness ratio of iron ore to coke layer, L_O/L_C, and so forth. Figure 1 shows the GUI menu in this model. Note that the descent of burden and the gas flow model will be included in later studies.

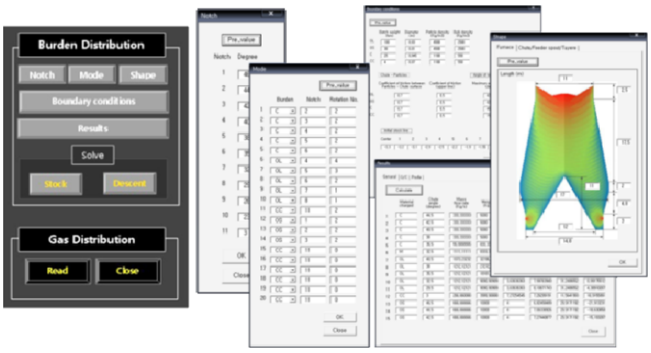

Fig. 1. GUI menu.

2.2. Burden trajectory

It is important to understand the behavior of the burden at each position of the charging equipment, because the burden will move consistently until it is stacked on top of the burden. To calculate the final burden trajectory, the velocity changes of the burden in the hopper, feeder spout, and the chute should be predicted.

The mass flow of the burden stored in the hopper is determined by the diameter of the orifice, and the burden is then moved to the feeder spout. However, the mass flow is set up in this model for convenience of the operator. When the burden discharged from the hopper passes the feeder spout due to gravity, the velocity of the particles decreases due to the inter-particle and particle to wall collisions. The equation for the particle velocity in the feeder spout, which follows Ideal Newton's law, is as follows [17],

$$V_{2v} = [V_{1v}^2 + 2GH_d]^{0.5} K_f \quad (1)$$

V_{1v}, V_{2v} = velocity at the entrance and exit of the feeder spout, respectively, m/s

H_d = height of feeder spout, m
K_f = correction factor for collisions

The particles discharged from the feeder spout are moved to the chute, and the particles are subject to four different forces during the chute transfer. The forces on the revolving chute are as follows [18].

1. Frictional force – parallel to the chute surface
2. Gravitational force – vertically downwards
3. Centrifugal force – in a tangential direction
4. Reactive force – perpendicular to the chute

The frictional force between the particle and the chute is differentiated by the type of material and the chute surface. The braking force is applied to consider the change of the particle velocity, which depends on the quality of the chute

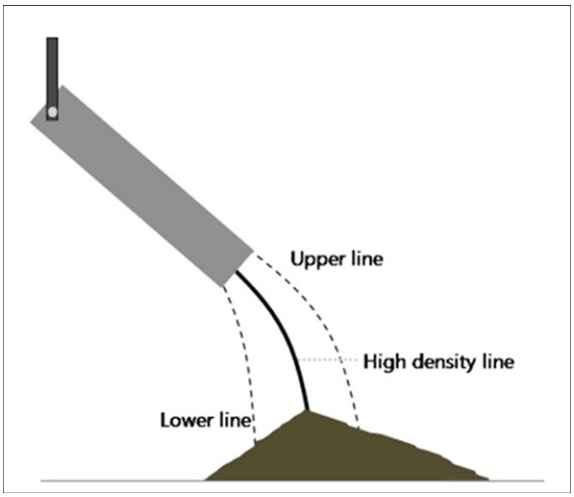

Fig. 2. Trajectory lines.

surface material [19]. When the burden falls, the frictional force, which is affected by the kinetic energy of each particle, is differentiated by the positions of particles on the chute surface. Therefore, in this model, the burden trajectory is divided into the upper and the lower lines, and the friction coefficient of each line is applied separately. Figure 2 shows the trajectory lines. The middle line between the two boundary lines is the high density flow, and it becomes the true burden trajectory. The equation for particle velocity in the chute exit is given below [17].

$$V_3 = [\omega^2\cos\alpha(\cos\alpha + \mu\sin\alpha)L^2\Phi^2 + 2g(\sin\alpha-\mu\cos\alpha)L^2\Phi + (V_{2v}\sin\alpha)^2]^{0.5} \quad (2)$$

ω = angular velocity, radian/s
μ = coefficient of friction between the particles and the chute surface
V_{2v} = velocity at the exit of the feeder spout, m
L = length of chute, m
α = acute angle between chute and horizontal, rad
Φ = correction factor

V_3 is decomposable to three formation factors, the radial, vertical, and tangential directions [17].

$$V_r = V_3\cos\alpha \quad (3)$$
$$V_z = -V_3\sin\alpha \quad (4)$$
$$V_\theta = r_c\omega \quad (5)$$

where r_c is the radius to the tip of the chute.

The trajectory lines were calculated based on the velocity of the burden, which was acquired via Eqs. 3 to 5. Only the vertical and horizontal compositions of the burden trajectory, without the tangential factor, were considered, because this model is a two-dimensional model. The trajectory is composed of the vertical and horizontal coordinates per unit time, and the relevant equations are given in Eqs. 6 and 7 [20].

Table 1. Variables for equation of angle of repose

Maximum angle of repose(deg.)	A_{max}
Diameter of particle(m)	D
Shape factor(-)	F_s
Diameter of throat(m)	d
Distance from center of a BF to trajectory line	X
Constant	C

$$X = V_3\cos\alpha \cdot t \quad (6)$$

$$Y = V_3\sin\alpha \cdot t + \frac{gt^2}{2} \quad (7)$$

t = time after leaving the chute tip, s
g = gravity acceleration, m/s^2

The angle of repose is the angle formed by the inclined plane with the horizontal surface such that the burden lying on the inclined plane is on the verge of sliding down along the inclined plane. This parameter, which massively influences the shape of the stock lines, usually increases as the particle size increases. The equation for the angle of repose based on the subdivided charging condition is necessary for the model development. In this model, the equation of the angle of repose is suggested from the results of the 1/5 and 1/12 scaled model experiments.

The variables applied to the mathematical analysis model are listed in Table 1. The angle of repose cannot exceed the maximum angle of repose that is measured by the 1/5 scaled model, and it is affected by the particle size and the shape factor. In Fig. 3, an additional factor exists in β, the outer angle of repose, since the angle of repose will decrease when the burden accumulates beside the wall. The burden falling position is added to consider this characteristic of the angle of repose. The final equations for the angle of repose include variables that are represented by

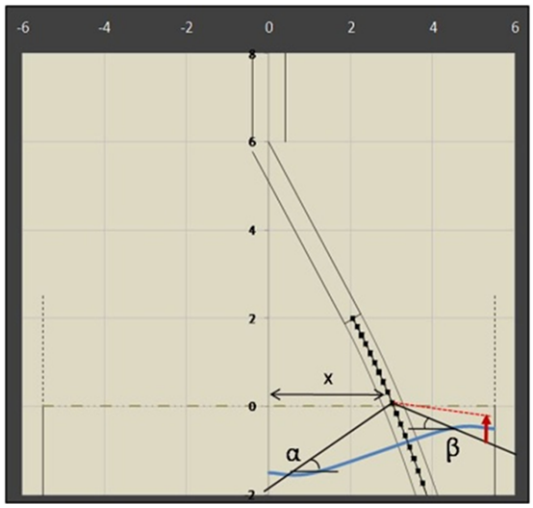

Fig. 3. Angle of repose, α and β.

Eqs. 8 and 9. The constant is used for modification of the equation, and the exponents are obtained by the scaled model results.

$$\alpha = A_{max} \cdot C \cdot \frac{D^{0.05}}{4 \cdot F_S^{0.05}} \quad (8)$$

$$\beta = A_{max} \cdot C \cdot \frac{D^{0.05}}{4 \cdot F_S^{0.05}} \cdot \frac{\frac{d}{2} - X^{1.4}}{5.8} \quad (9)$$

2.3. Burden distribution

2.3.1. Formation of stock lines

The burden profile is represented by a radial surface stock line, and is calculated from the burden trajectory. The formation of the stock line was composed of two stages. The primary stage of stock line formation was performed by setting up the primary stock line (SL_1) through surface measurement of a blast furnace operation. The burden is then stacked on the upper boundary of the primary stock line, and charging of the first batch proceeds through the charging mode. Each stock line is created with an angle of repose from the high density flow of the burden trajectory from the analysis model. Also, the area among stock lines is converted to volume, and calculated in the same manner as the real charging volume for calculation of a layer thickness. After the completion of burdening, the upper boundary line of the layer becomes the second stock line (SL_2) in Fig. 4. In the secondary stage, the second stock line (SL_2) is lowered to level h, and becomes the third stock line (SL_3). The h value should be set up independently for better calculation results. The fourth stock line (SL_4) based on the third stock line (SL_3) is developed by the same method as used in the primary stage.

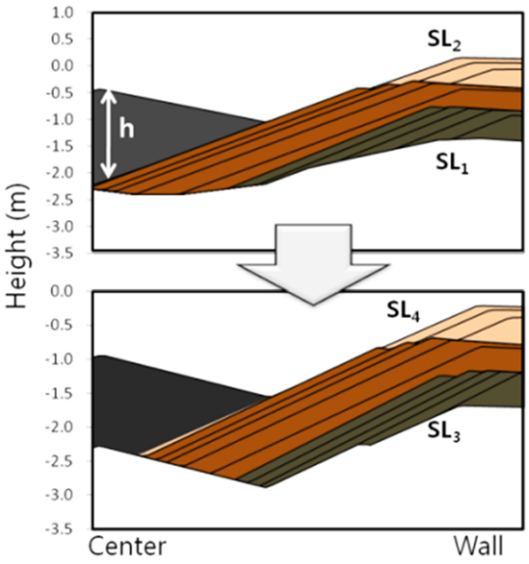

Fig. 4. The formation of stock lines.

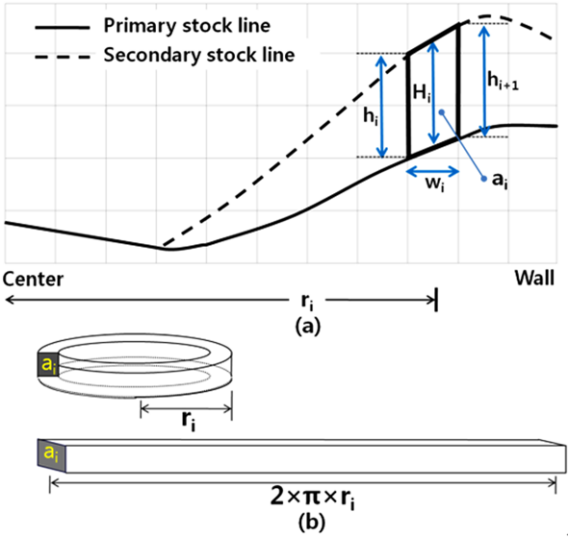

Fig. 5. The method to convert area into volume.

It is important to decide the height of the stacked layer for calculation of the stock line. As presented in Fig. 4, each stock line is formed by the charging mode, and the height of each stacked layer is subsequently determined. For comparison with the real charging volume, it is necessary to convert the area into volume, because the present analysis model is a 2-dimensional model.

Figure 5 shows the method for calculating the height of each layer. First, the secondary stock line is formed on the primary stock line. The shape of the secondary stock line is fixed but it is possible to move to perpendicular. The layer area surrounded by the primary and secondary stock line is divided into different areas such as a_i. The area of a_i can be calculated by Eq. 10.

$$a_i = \frac{h_i + h_{i+1}}{2} \cdot W_i \quad (10)$$

In Fig. 5(b), a_i is converted to volume (V_i) by axial rotation. The volume of a ring, V_i, and the total volume surrounded by the primary and secondary stock line, V_{total}, are calculated by Eqs. 11 and 12.

$$V_i = a_i \cdot 2 \cdot \pi \cdot r_i \quad (11)$$

$$V_{total} = \sum_{i=1}^{140} V_i \quad (12)$$

V_{total} is changed by the distance that the secondary stock line moves vertically until satisfying the iteration criterion, which is the gap between V_{total} and the real charging volume, within a specified tolerance. The height of the layer is then decided.

The burden profile calculated by this model is used for the analysis of gas flow. Each section of Fig. 6(a) was separated into cells that contain information of the burden type, as shown in Fig. 6(b). Each cell contains information

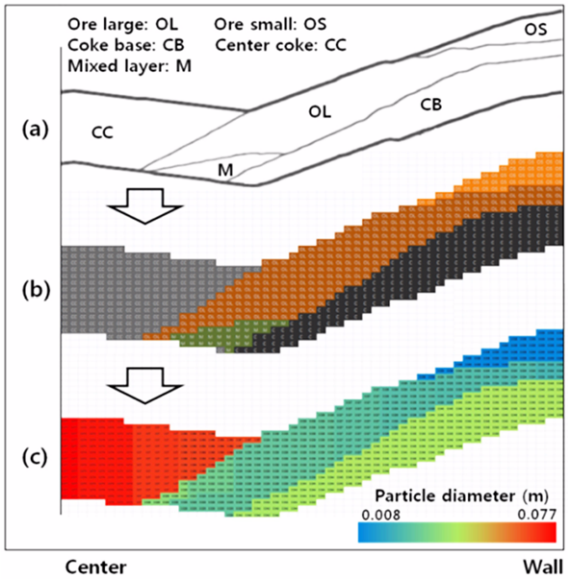

Fig. 6. The conversion of burden profile into cells.

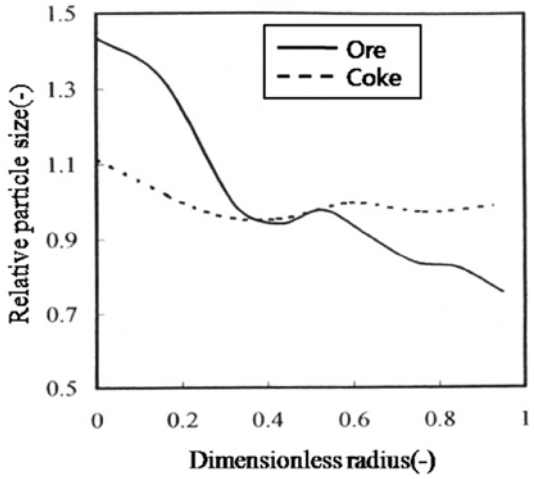

Fig. 7. Particle size distribution in the radial direction.

such as diameter, porosity, and shape factor. The variables can be used for Ergun's equation, which calculates the pressure drops of injected gasses. Figure 6(c) shows the particle size distribution with respect to the radial direction. In this model, the radial distribution of the particle size was considered with the data of Fig. 7 [20].

Table 4. The burden properties used for the analysis model

	Diameter(m)	Density(Kg/m^3)	Shape factor
O_L	0.03	2500	0.77
O_S	0.01	2500	0.61
C_B	0.05	550	0.81
C_C	0.07	550	0.89

The burden profile was compared according to the charging pattern for verification of the change of the stock profile calculated by the analysis model. The charging pattern is listed in Table 2, and the notch angle and burden properties are listed in Tables 3 and 4.

2.3.2. Mixed layer formation

The mixed layer formation due to collapse of the coke layer affects the permeability, because the properties of the mixed layer such as porosity and particle size are different from those of the original burden type. As a general method for addressing mixed layer formation, according to Inada *et al.* [4], the extent of mixed layer formation can be linearly expressed by the "formation energy of mixed layer". The formation energy includes the collision energy of ore and the potential energy of ore at the falling position of ore, and it affects the thickness of the mixed layer.

In this study, the analysis of mixed layer formation was approached by the angle of repose and the volume of mixed layer. The mixed layer is created when the iron ore is only charged on the coke layer. The volume of iron ore and coke particles that is moved to the center part of the BF by collapse of the coke layer is identical to the reduced volume of two layers, the upper layer of coke base and the bottom layer of iron ore. The volumetric ratio of iron ore and coke was fixed, and the 1/12 scaled model and DEM simulation were used for calculation of the total volume and the angle of repose of the mixed layer.

Table 2. The charging pattern used for the analysis model

	Mode															Batch weight(ton)				O/C
		C					O_L					C_C		O_S						
Case 1	Notch	4	5	6	7	8	2	3	4	5	6	11	1	2	3	O_L	O_S	C	C_C	4.61
	Revolution	2	2	2	2	2	4	3	2	1	1	2	2	2	2	100	30	25	4	
Case 2	Notch	2	3	4	5	6	4	5	6	7	8	11	1	2	3	O_L	O_S	C	C_C	4.61
	Revolution	2	2	2	2	2	4	3	2	1	1	2	2	2	2	100	30	25	4	
Case 3	Notch	2	3	4	5	6	4	5	6	7	8	11	1	2	3	O_L	O_S	C	C_C	2.83
	Revolution	2	2	2	2	2	4	3	2	1	1	2	2	2	2	90	27	35	7	

Table 3. The charging notch of a chute

Notch	1	2	3	4	5	6	7	8	9	10	11
Angle(deg.)	47	45	43	41	38	36	33	30	26	23	3

2.4. DEM (Discrete element method)

For the development of advanced mathematical models of a BF, the DEM (Discrete Element Method) has attracted special attention in the iron-making field. Moreover, a combined model of a DEM with the continuum model is under development for the purpose of arriving at an accurate understanding of the inner state of the blast furnace. In the continuum model, the solid motion is generally derived from the quasi-fluid equation based on the expansion of kinetic theory. On the other hand, in the DEM, Newton's 2nd law is applied for each particle [21]. Since the motion of the particle is not averaged in the DEM, discontinuous phenomena can be precisely represented. However, the object of the DEM is limited to the condensed phase. Various types of contact between particles are evaluated in the DEM, and the movement of each particle is then decided. The computational load of the discrete model is consequently extremely large compared to the continuum model [22].

In this study, EDEM® software, developed by DEM solutions Ltd, was used for modification of the analysis model. For a realistic analysis of the falling behavior of particles, particles were traced from the bunker to the stacked surface, and the particle size distribution was considered. Boundary conditions of the EDEM simulation of charging burden are listed in Table 5. The tilting angle is fixed at 45°, and the velocity of revolution is 8rpm. Also, ten thousand coke particles were used for the calculation.

Table 5. Boundary conditions used for EDEM simulation of charging burden

Tilting angle	45° (degree)
Velocity of revolution	8 rpm
Ore type	Coke
The number of particles	10000
Particle diameter	3~7 mm

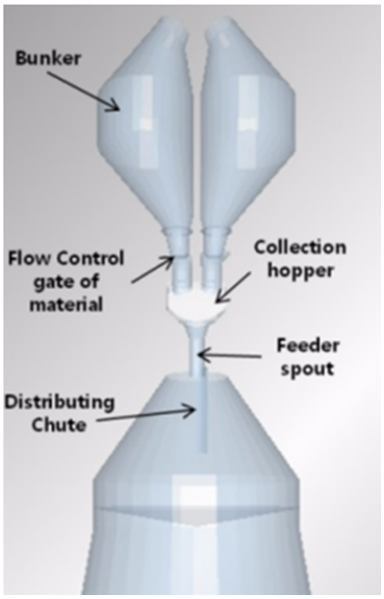

Fig. 8. The shape of a BF for analysis of falling trajectory by use of the EDEM.

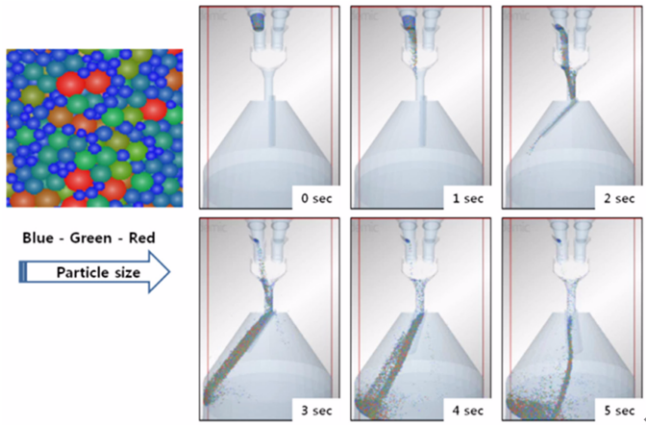

Fig. 9. The particle behavior in the charging equipment of a BF.

Figure 8 shows the shape of the BF considered in the EDEM simulation. The bunker, flow control gate, collection hopper, feeder spout and distributing chute are simulated as a real BF.

Figure 9 shows the particle behavior according to time in the charging equipment. The particles, which are classified according to particle size with colors and charged in one of the bunkers, move through the charging equipment. Since

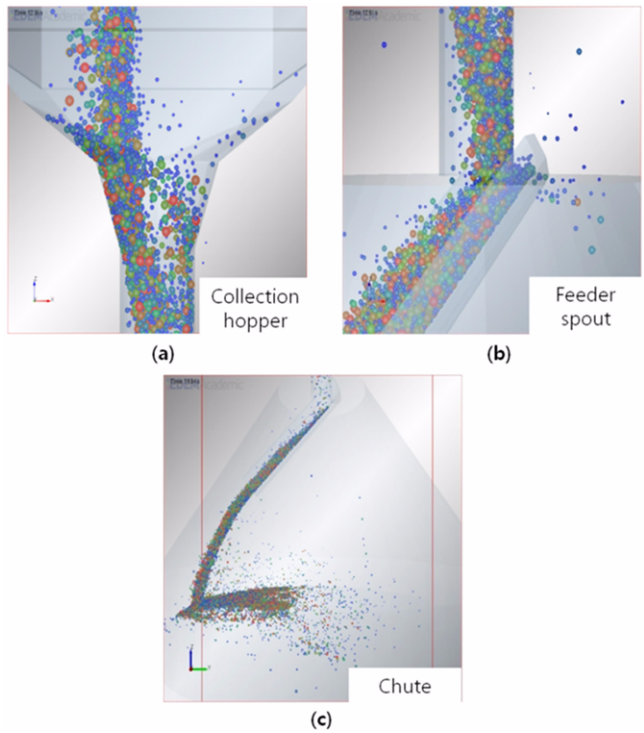

Fig. 10. The particle behavior in the charging equipment.

Fig. 11. Geometry for analysis of mixed layer by use of the EDEM.

the geometry for the analysis of the falling trajectory is the same as that of a real BF and individual particles are calculated, the falling trajectory is accurately calculated. Figure 10 shows a magnified view the particle behavior in the collection hopper, feeder spout, and chute. Since only one hopper is used when the particles are charged, the particle flow is concentrated to one side in the collection hopper and this affects the particle behavior in the feeder spout and chute. Also, the width and particle size distribution of the falling trajectory are obtained by the EDEM simulation.

The formation of a mixed layer was also calculated by the EDEM. The calculation of individual particles makes it possible to confirm the formation of a mixed layer and the ratio of the volume of the iron ore and the coke in the mixed layer for development of the analysis model. For simplicity, the furnace shape is assumed to be a two-dimensional flat-type in order to decrease the particle numbers. The chute can move only vertically because the thickness of the geometry is 200 mm, as seen in Fig. 11. The mean particle size of iron ore, coke, and center coke used in the calculations are 16 mm, 20.5 mm, and 33 mm, respectively. The notch angle and the charging pattern are listed in Tables 3 and 6.

3. EXPERIMENTAL METHOD

3.1. 1/5 scaled model

The equations for the angle of repose were developed by the scaled model, with particular emphasis on the 1/5 scaled model. In that model, the inner and outer angle of repose, α and β, were measured to assess the change of the angle of repose according to the tilting angle. The boundary conditions of the 1/5 scaled model are listed in Table 7. The length and diameter of the chute are 0.9 m and 0.2 m, respectively, and the distance from the bottom to the chute tip is 0.5 m when the tilting angle of the chute is zero. The angle of repose of the iron ore and coke are then measured. The burden property according to the burden type is listed in Table 8.

The results of angle of repose in the 1/5 scaled model experiment according to the tilting angles, which are 0°, 30°, 35°, 40° and 45°, are listed in Table 9. In all five cases, the angle of repose decreases with an increase of the tilting angle. In addition, the outer angle of repose, β, was smaller than α, since the moving distance of particles that move to the outer part due to kinetic energy is greater than that to the inner part.

The particle size and shape factor mostly affect the angle of repose. In this experiment, the particle size and shape factor of coke are greater than those of ore, and thus the angle of repose of coke was measured to be larger than that of ore. The maximum angle of repose of the ore and coke,

Table 7. Boundary conditions of a 1/5 scaled model experiment

Scale	1 : 5
Length of chute (m)	0.9
Diameter of chute (m)	0.2
Height from bottom to chute tip (m)	0.5
Particle diameter (mm)	Ore: 4, Coke: 8
Shape factor	Ore: 0.7, Coke: 0.85
Charging weight (Kg)	Ore: 25, Coke: 12
Tilting angle of chute (degree)	0, 30, 35, 40, 45

Table 8. The burden properties used for the scaled model experiment

	Diameter(m)	Density(Kg/m^3)	Shape factor
O_L	0.006	2500	0.77
O_S	0.003	2500	0.61
C_B	0.007	550	0.81
C_C	0.010	550	0.89

Table 6. Charging pattern for EDEM simulation

	Mode											Batch weight (ton)		
	C_B					O_L					C_C			
Notch	2	3	4	5	6	3	4	5	6	7	11	C_B	O_L	C_C
Revolution	3	3	3	3	3	4	4	2	1	1	2	25	66	5

Table 9. The result of angle of repose in a 1/5 scaled model experiment

		0°	30°	35°	40°	45°	Average	Maximum angle of repose
Ore	α	35.4	31.2	30.5	30.1	29.5	31.34	35.3
	β	35.1	14.1	13.8	13.5	13.1	17.92	
Coke	α	38.2	36.8	34.2	33.3	32.3	34.96	38.4
	β	38.5	16.1	14.5	13.9	13.8	19.36	

Table 10. The charging pattern used for the scaled model

	Mode														Batch weight(ton)				O/C
	C_B					O_L					C_C		O_S						
Notch	2	3	4	5	6	4	5	6	7	8	11	1	2	3	O_L	O_S	C_B	C_C	4.5
Revolution	2	2	2	2	2	4	3	2	1	1	2	2	2	2	8.3	2.5	2.1	0.3	

measured when the tilting angle is zero, is 35.3 and 38.4, respectively. The data of the 1/5 scaled model were applied to the equation of the angle of repose.

3.2. 1/12 scaled model

The burden distribution was calculated, and the results were compared with those of the 1/12 scaled model experiment to check its validity. The notch angle and charging pattern are listed in Tables 3 and 10. The burden was charged in the order of the coke base (C_B), ore large (O_L), ore small (O_S), and center coke (C_C). In the apparatus, the burden descends via the lift during charging.

4. RESULTS AND DISCUSSION

4.1. Charging burden

The burden trajectory was calculated by the analysis model developed by the scaled model and kinetic equations. Initial boundary conditions, such as charging pattern, notch angle, and batch volume, used in real operations were utilized. The burden trajectory was calculated while taking into account the frictional force between particles and between particles and the chute and the turning force of chute.

First, the velocity of burden was calculated at the chute tip according to variables such as RPM, chute angle, and length of chute. Figure 12 shows the velocity change as a function of the variables. On the basis of comparison with other numerical models, the results can be considered as reasonable data, and they were used to determine the burden trajectory and angle of repose.

The results of the falling trajectory of the coke with a tilting angle of 44.4° obtained by the present scaled model experiment were compared with those calculated by EDEM and the analysis model. In the scaled model, the trajectory was analyzed by images of falling particles, and in the analysis model and EDEM, the burden trajectory was calculated under the same conditions as employed for the

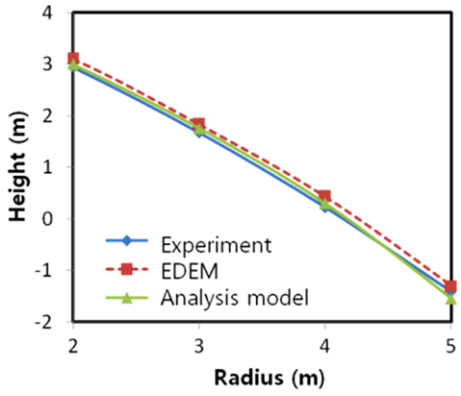

Fig. 13. Experiment-DEM-Model comparison of trajectory for dumping of coke at a chute angle setting of 44.4°.

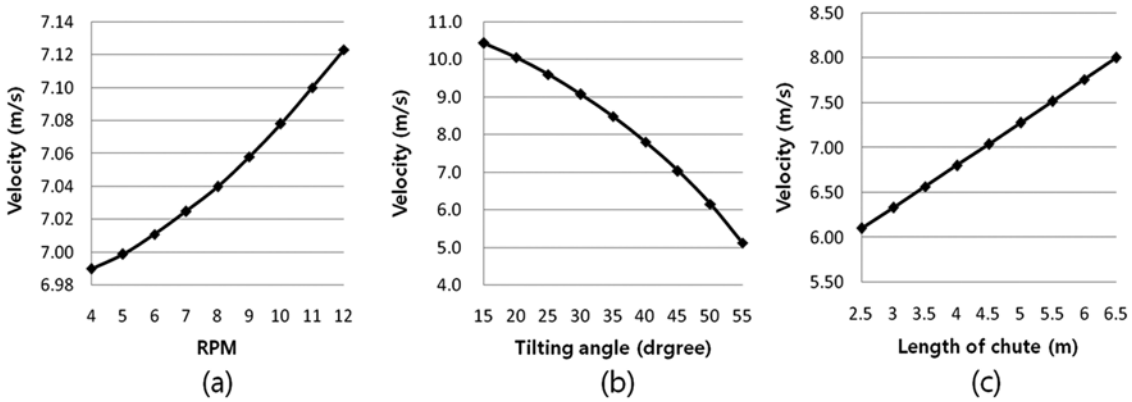

Fig. 12. The change of particle velocity at chute tip according to variables.

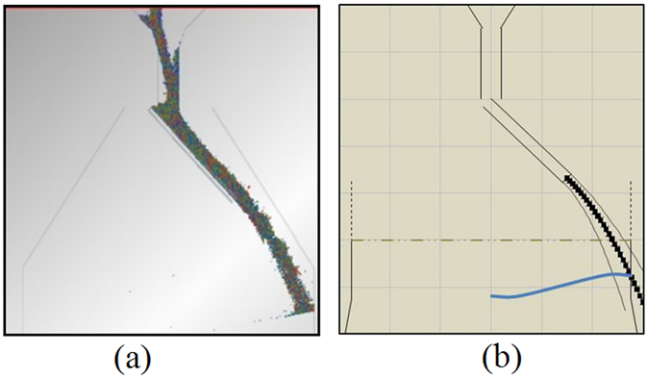

Fig. 14. Trajectory for dumping of coke at a chute angle setting of 44.4° (a) by EDEM, and (b) The analysis model.

scaled model. In the analysis model, the friction coefficient was adjusted by the scaled model experimental data. Figure 13 presents comparisons of the burden trajectory with the scaled model, EDEM, and the analysis model, revealing good agreement.

Figure 14 provides a comparison of the results of EDEM and the analysis model. Since the analysis model was modified by the EDEM and the scaled model, the two sets of results are similar. In the analysis model, the shape of the BF and the burden trajectory were expressed graphically, and therefore it is possible to respond immediately when the furnace shape and burden trajectory change.

The falling trajectories of iron ore and coke were compared via the analysis model with the tilting angles of 46°, 40°, 32°, 23°, and 8°. In Fig. 15, the moving distance from the center of the BF becomes greater as the tilting angle increases. However, the distance from the chute tip becomes smaller, because the particle velocity decreases with an increase of frictional force when the tilting angle is more than 40°. From the comparison of iron ore and coke,

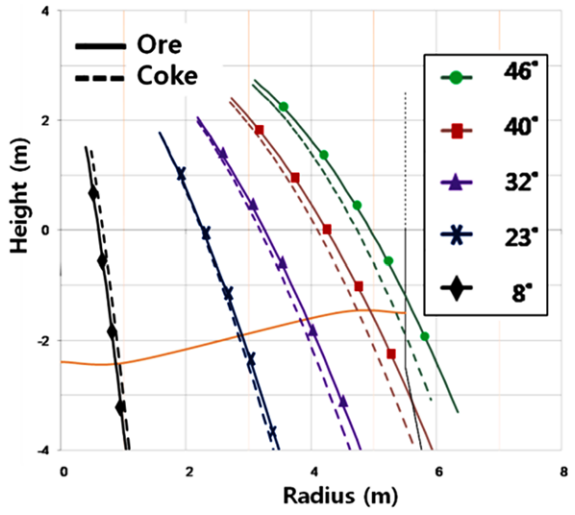

Fig. 15. Ore-coke comparison of trajectory.

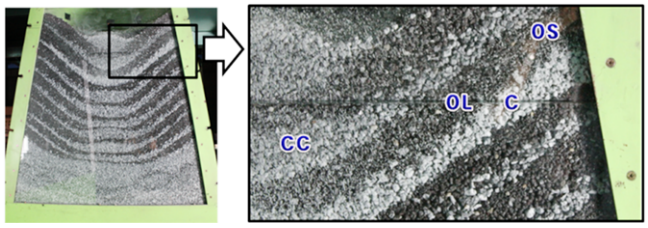

Fig. 16. The burden profile in the 1/12 scaled model experiment.

excluding the 8 degree angle case, the moving distance of the iron ore was greater than that of coke. Different friction coefficients are applied according to burden type, and the results corresponded with the experimental results.

4.2. Radial burden profile

Figure 16 shows the burden distribution in the 1/12 scaled model. An acrylic board was situated in the cross section to observe the stock profile in the experimental apparatus. This could lead to different conditions when the burden is stacked, because the acrylic board interferes with the falling burden. Coke was colored white to differentiate if from iron ore.

Figure 17 shows a comparison of the burden stock lines of the scaled model with the calculations. A laser profile meter was used to measure the burden profile in the radial direction after each charging. The mixed layer placement cannot be measured by the laser in the scaled model, because the laser only measures the upper part of the burden. Therefore, the mixed layers calculated from the analysis model and the experimental results were not comparable. The results of the analysis model are similar to the scaled model due to modification of the mathematical formula, and thus it was possible to obtain more accurate calculation results.

The kinetic energy of iron ore leads to collapse of the coke layer as the heavy iron ore falls. The collapsed coke will move to the center of the BF, and a mixed layer will be created. The density of the mixed layer will be determined by the mixing ratio of coke to iron ore. The volumetric ratio of coke is known to be in the range of 25 % to 75 % in the mixed layer. Figure 18 presents experimental results showing the formation of the mixed layer when iron ore is stacked at the top of the coke layer. The coke layer is tran-

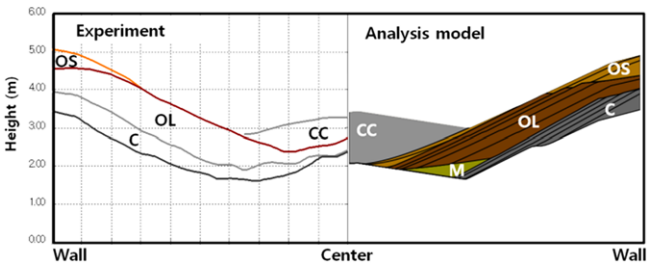

Fig. 17. Comparison of model result with experimental result.

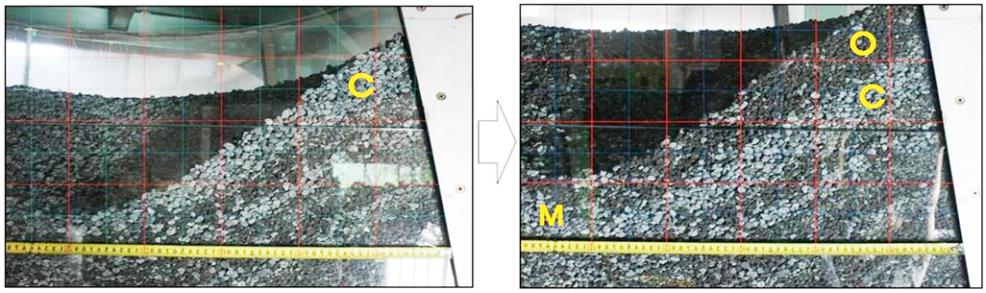

Fig. 18. The change of coke layer and mixed layer formation.

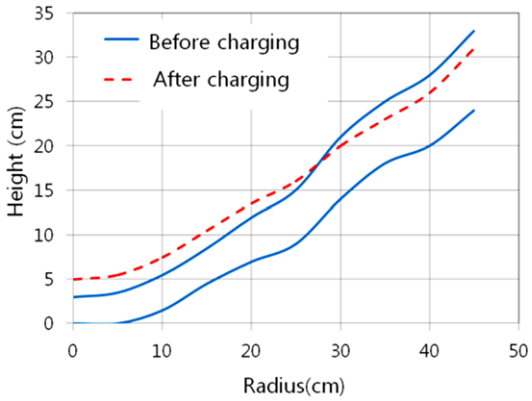

Fig. 19. The change of coke layer surface profile.

sited to the center of the furnace via collisions with the iron ore. Also, the coke particles that move to the center and the iron ore particles are mixed, and form a mixed layer. Figure 19 shows the change of the coke layer.

Figure 20 shows the change of the burden layer as determined by the EDEM simulation when iron ore is stacked on the top of the coke based layer. The particles on the coke layer moved toward the center because of the kinetic energy of high density iron ore, similar to the experimental results. Figure 20(b) shows a comparison of the upper line of the coke layer before and after ore charging. A notable change in the burden layer is easily seen.

Figure 21 shows a magnified view of the mixed layer after iron ore charging. The particles of iron ore and coke slid down the slope and mixed together. Five lines were set up in the radial direction, and the volumetric ratio between iron ore and coke was calculated. The volumetric ratio result was 0.456 for iron ore and 0.534 for coke, and these values were used in the analysis model.

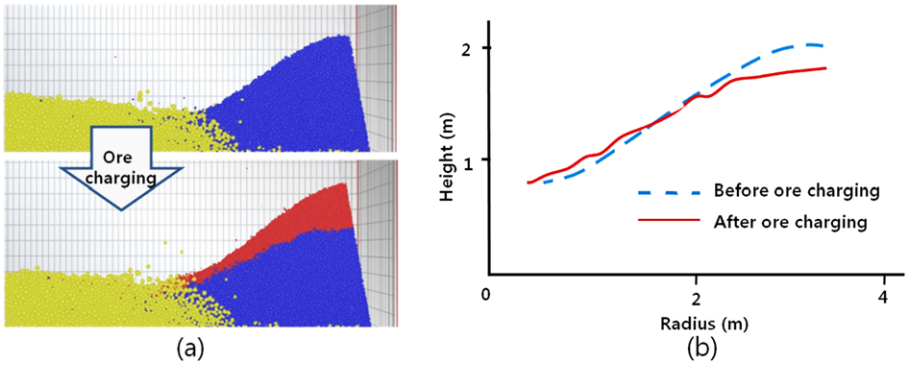

Fig. 20. (a) The EDEM result of change of coke layer and the mixed layer formation, and (b) the change of coke stock line.

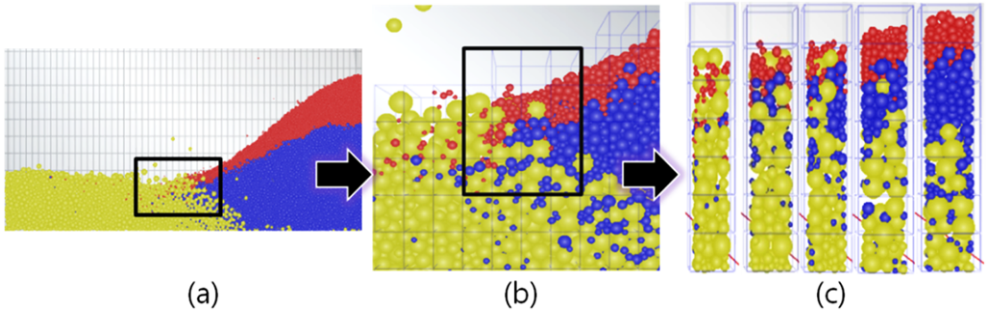

Fig. 21. The particle size distribution in mixed layer.

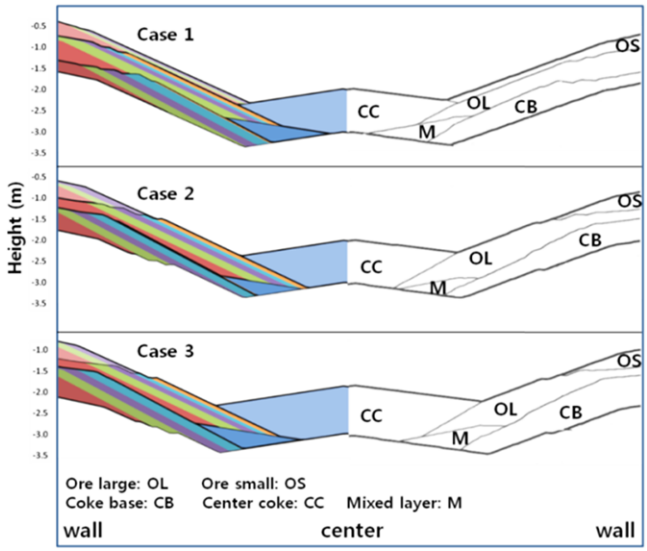

Fig. 22. Burden profile calculated by use of a analysis model.

For verification of the change of the stock profile according to the charging pattern, the burden profile was compared when the charging pattern and weight percent of the burden were changed. The charging pattern in CASE 1 and the weight percent of burden in CASE 3 were changed from the standard, CASE 2. The charging pattern for the analysis of the burden distribution is listed in Table 2, and the notch angle and burden properties are listed in Tables 3 and 4. Figure 22 shows the calculated burden profile. A layer is composed of 5 parts, which are ore large, ore small, coke base, center coke, and mixed layer.

In CASE 1, the coke base layer is moved relatively closer to the center and the thickness of the ore layer becomes greater at the side region, as compared with CASE 2, due to the change of the charging pattern. In CASE 1, the coke notch number increased and the notch number of ore large became smaller than that of CASE 2.

In Fig. 23, the graph shows the depth ratio of iron ore and coke. In CASE 2, L_O/L_C is below 3 and is high in the middle of the radius. However, L_O/L_C of CASE 1 shows a relative increase according to the radius direction. When CASE 3 was compared with CASE 2, the thickness of the coke layer increased more due to the increase of the weight percent of coke, which has a low density. In the graph, L_O/L_C of CASE 3 is lower than that of CASE 2 overall.

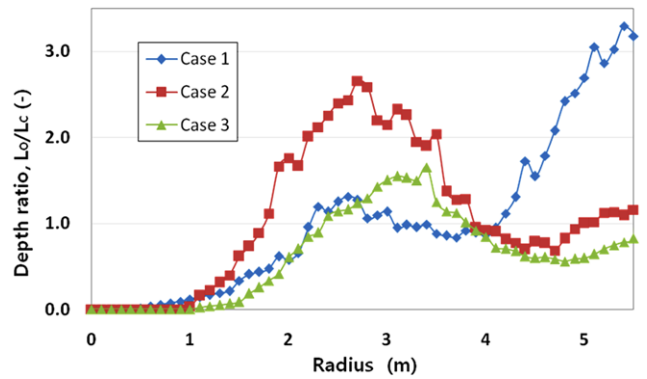

Fig. 23. Depth ratio at the upper part.

5. CONCLUSIONS

In this study, an analysis model for the burden distribution was developed from mathematical modeling, and it was used for calculation of the burden trajectory and stock line. The results of mathematical formula for the analysis of the burden behavior were compared with those of a scaled model experiment and EDEM simulation to determine the effectiveness of the proposed model.

Initial boundary conditions, such as charging pattern, notch angle, and batch volume, used in real operations were utilized. The burden trajectory was calculated while taking into account the frictional force between particles and between particles and the chute and the turning force of chute. The burden trajectories from the analysis model, scaled model, and EDEM yielded similar results.

The stock layer made by 15 to 20 stock lines was calculated by the change of the angle of repose and the calculation of layer height. A layer is composed of 5 parts, which are ore large, ore small, coke base, center coke, and mixed layer. The change of the burden profile was compared when the charging pattern and weight percent of the burden were changed. The burden profile was affected by variation of these parameters, and was similar to the profile obtained through a scaled model experiment. The burden profile calculated by this model will be used for the analysis of burden descent and gas flow.

ACKNOWLEDGMENTS

This work was partially supported by the technical research center, Hyundai steel company.

REFERENCES

1. R. Goffin, *Blast Furnace Burden Distribution–Principles and Practices*, -1, Iron and Steel Society, Nashville (1995).
2. Y. Okuno, K. Kunitomo, T. Irita, and S. Matsuzaki, *Tetsu-to-Hagané* **72**, 783 (1986).
3. Y. Okuno, S. Matsuzaki, K. Kunitomo, M. Isoyama, and Y. Kusano, *Tetsu-to-Hagané* **73**, 91 (1987).
4. T. Inada, Y. Kajiwara, and T. Tanaka, *49th Ironmak. Conf. Proc.*, p. 263, Iron and Steel Society, Warrendale, PA (1990).
5. K. Okimoto, S. Inaba, R. Ono, and M. Takada. *Tetsu-to-Hagané* **71**, A9 (1985).
6. J. J. Povermo, *Blast Furnace Burden Distribution-Princi-*

ples and Practices, p. 1, Iron and Steel Society (1995).
7. P. L. Hooey, A. Boden, C. Wang, C. Grip, and B. Jansson, *ISIJ Int.* **50**, 924 (2010).
8. P. R. Austin, H. Nogami, and J. Yagi, *ISIJ Int*. **37**, 458 (1997).
9. P. R. Austin, H. Nogami, and J. Yagi, *ISIJ Int*. **37**, 748 (1997).
10. P. R. Austin, H. Nogami, and J. Yagi, *ISIJ Int*. **38**, 10 (1998).
11. J. A. Castro, H. Nogami, and J. Yagi, *ISIJ Int*. **42**, 44 (2002).
12. T. Sugiyama and M. Sugata, *Seitetsu Kenkyu* 34 (1987).
13. K. Takatani, T. Inada, and Y. Ujisawa, *ISIJ Int*. **39**, 15 (1999).
14. S. Natsui, S. Ueda, M. Oikawa, Z. Fan, J. Kano, R. Inoue, and T. Ariyama, *ISIJ Int.* **49**, 1308 (2009).
15. Robert de Levie, *Advanced Excel for Scientific Data Analysis*, Oxford University Press (2004).
16. D. M. Bourg, *Excel Scientific and Engineering Cookbook*, O'Reilly (2006).
17. V. R. Radhakrishnan and K. M. Ram, *J. Proc. Control.* **11**, 565 (2001).
18. N. Standish, *Principles of Burdening and Bell-Less Charging*, Nimaroo Publishers, Wolloongong, Australia (1989).
19. T. Nagai, *Mc Master Symposium on Optimum Burden Distribution in Blast Furnace*, 13.1 (1978).
20. S. K. Jung, C. Y. Beak, and W. S. Chung, *J. Kor. Inst. Met. & Mater*. **39**, 1171 (2001).
21. P. A. Cundall and O. D. L. Strackm, *Geotechnique* **29**, 47 (1979).
22. S. Ueda, S. Natsui, H. Nogami, J. Yagi, and T. Ariyama, *ISIJ Int*. **50**, 914 (2010).